Theory of Time-Dependent Reactive Scattering: Cumulative Time-Evolving Differential Cross Sections and Nearside−Farside Analyses of Time-Dependent Scattering Amplitudes for the H + D_2 → HD + D Reaction†

P. D. D. Monks and J. N. L. Connor*

School of Chemistry, The University of Manchester, Manchester M13 9PL, England

S. C. Althorpe

Department of Chemistry, University of Cambridge, Lensfield Road, Cambridge CB2 1EW, England

Received: October 3, 2005

Nearside−farside (NF) theory, originally developed in the energy domain for the time-independent description of molecular collisions and chemical reactions, is applied to the plane wave packet (PWP) formulation of time-dependent scattering. The NF theory decomposes the partial wave series representation for the time-dependent PWP scattering amplitude into two time-dependent subamplitudes: one N, the other F. In addition, NF local angular momentum (LAM) theory is applied to the PWP scattering amplitude. The novel concept of a cumulative time-evolving differential cross section is introduced, in which the upper infinite time limit of a half-Fourier transform is replaced by a finite time. In a similar way, a cumulative energy-evolving angular distribution is defined. Application is made to the state-to-state reaction, H + $D_2(v_i = 0, j_i = 0)$ → HD(v_f = 3, $j_f = 0$) + D, where v_i, j_i and v_f, j_f are vibrational and rotational quantum numbers for the initial and final states, respectively. This reaction exhibits time-direct and time-delayed (by about 25 fs) collision mechanisms. It is shown that the direct-time mechanism is N dominant scattering, whereas the time-delayed mechanism exhibits characteristics of NF interference. The NF and LAM theories provide valuable insights into the time-dependent properties of a reaction, as do snapshots from a movie of the cumulative time-evolving differential cross section.

1. Introduction

Theories of time-dependent (wave packet) and time-independent (energy-domain) scattering provide well-established procedures for understanding the dynamics of chemical reactions (for recent reviews of the literature, see refs 1−5). A recent development[6−12] is a general *plane wave packet (PWP)* theory of elastic, inelastic, and reactive scattering (reviewed in ref 13). It uses time-evolving wave packets to provide a physically transparent visualization—including movies—for the results from energy-domain scattering calculations (and experiments). It does this by locating a PWP in the entrance channel at the closest distance for which the interaction potential is negligible, letting the wave packet evolve in time, and then projecting onto a probe PWP in the exit channel, again at the closest distance where the interaction potential can be neglected.[6−13] The PWP theory builds on earlier research using wave packets for reactive scattering, e.g., refs 14−17.

The PWP formulation provides, with the help of an energy filter, a time-evolving visualization of a *differential cross section* that has been computed from a time-independent scattering theory. Furthermore, the PWP theory uses concepts analogous to those employed in time-independent scattering theory. For example, the PWP theory employs time-evolving concepts such as: time-dependent angular distributions, a partial wave series representation of the time-dependent scattering amplitude, and time-dependent scattering matrix elements.[6−13]

Another development in scattering theory in the energy-domain has been the introduction of *nearside−farside (NF)* methods[18−47] to analyze the complicated interference patterns often observed in differential cross sections under semiclassical conditions, i.e., when the partial wave series for the scattering amplitude contains a large number of numerically significant terms. NF theory decomposes the scattering amplitude exactly into a N subamplitude plus a F subamplitude, which have simpler properties than the full amplitude. Structure in the angular scattering can then arise from the N subamplitude, or from the F subamplitude, or from interference between the N and F subamplitudes (for reviews, see refs 5, 45, 48). Recently, the concept of a *local angular momentum (LAM)* has been introduced,[35,36,38,40] which further extends the usefulness of NF techniques for understanding the dynamics of molecular collisions.

The purpose of this paper is to apply NF and LAM theory (originally developed and applied in the energy-domain) to the PWP time-evolving description of chemical reactions. The theoretical methods used in this paper are discussed in section 2. We consider the time-dependent scattering amplitude, its expansion in a Legendre partial wave series, time-dependent scattering matrix elements and the time-dependent angular distribution. We also discuss the Fourier transform relation between these time-dependent quantities and the corresponding time-independent quantities. Section 2 also introduces the novel concepts of a *cumulative time-evolving differential cross section* and a *cumulative energy-evolving angular distribution* for which upper infinite limits of half-Fourier transforms are replaced by finite values. Finally we describe how to NF and LAM analyze the time-dependent scattering amplitude.

The theory developed in section 2, parts A−D, of this paper is for a general state-to state reaction of the type

† Part of the special issue "Donald G. Truhlar Festschrift".

10.1021/jp0556254 CCC: $33.50
Published on Web 12/22/2005

$$A + BC(v_i, j_i, m_i) \rightarrow AB(v_f, j_f, m_f) + C$$

where v_i, j_i, m_i and v_f, j_f, m_f are the vibrational, rotational and helicity quantum numbers for the initial and final states, respectively. We apply the theory in section 3 to the reaction

$$H + D_2(v_i = 0, j_i = 0, m_i = 0) \rightarrow HD(v_f = 3, j_f = 0, m_f = 0) + D$$

Since both helicity quantum numbers are zero, the time-dependent scattering amplitude can be expanded in a basis set of Legendre polynomials (section 2E), which leads to a simpler development of the NF and LAM theory in section 2, parts F and G. Our results for the $H + D_2$ reaction are described and discussed in section 4. Our conclusions are given in section 5.

We have chosen the $H + D_2$ reaction because a recent study[6] has clearly identified two distinct mechanisms for this reaction (see also, refs 1, 37, 44−46, and 49). One is a direct-recoil mechanism, in which H approaches D_2 in a mainly collinear configuration, resulting in HD being scattered into the backward direction relative to the direction of the incoming H atom. The other mechanism is dominated by HD being scattered into the forward direction and is due to a slow down in the translational motion of the intermediate complex near the reaction barrier, resulting in a time delay of approximately 25 fs relative to the time-direct mechanism.[6,49] (A complementary explanation can be given in terms of decaying Regge states[37,44−46]). These time-direct and time-delayed mechanisms offer an excellent opportunity to make a detailed study of a chemical reaction from a time-dependent point of view.

2. Theoretical Methods

A. Introduction. Our starting point is the energy dependent-scattering amplitude, $f(\theta_R,E)$, where E is the total energy and θ_R is the reactive scattering angle, i.e., the angle between the outgoing AB molecule and the incoming A atom. It is also convenient for the following analysis to choose $E = 0$ so that $f(\theta_R,E) \equiv 0$ for $E < 0$, i.e., the reactive scattering channel, v_i, j_i, $m_i \rightarrow v_f$, j_f, m_f is closed when $E < 0$. There are many computational methods in the literature for calculating $f(\theta_R,E)$ over a (finite) range of E values.[1−5] The energy-dependent differential cross section is given by

$$\sigma(\theta_R,E) = |f(\theta_R,E)|^2 \qquad (2.1)$$

Remarks:

(a) We have omitted the label v_i, j_i, $m_i \rightarrow v_f$, j_f, m_f from $f(\theta_R,E)$, $\sigma(\theta_R,E)$ and similar quantities in this paper to keep the notation simple.

(b) It is common, as is done in sections 3 and 4, to measure E for a state-to state chemical reaction from the classical minimum of the BC potential energy curve. Then the state-to-state reactive scattering channel is closed for $E < E_{threshold}$, where $E_{threshold} > 0$ is the larger of the rovibrational energies of $BC(v_i, j_i)$ and $AB(v_f, j_f)$.

B. Time-Dependent Scattering Amplitude. We define a time-dependent scattering amplitude, $f(\theta_R,t)$, where t is the time, by the half-Fourier transform[11,12]

$$f(\theta_R,t) = \int_0^\infty F(E) f(\theta_R,E) \exp(-iEt/\hbar)\, dE \qquad \text{(N.B., dimensions = length} \times \text{energy)} \quad (2.2)$$

In eq 2.2, $F(E)$ is a dimensionless complex-valued energy filter function,[11,12] which is chosen to extract interesting information from $f(\theta_R,E)$ and map it to the time domain as given by $f(\theta_R,t)$. The filter function used in section 3 has the property $F(E) \rightarrow 0$ as $E \rightarrow \infty$. Note that different choices for $F(E)$ will generate different $f(\theta_R,t)$.

It is also convenient in eq 2.2 to choose $t = 0$ as a time before A and BC have interacted. We can then assume $f(\theta_R,t) \equiv 0$ for $t < 0$. As t increases in eq 2.2, the exponential factor in the integrand will oscillate faster and faster, and $f(\theta_R,t) \rightarrow 0$ as $t \rightarrow \infty$ by the Riemann-Lebesgue Lemma[50] [assuming $F(E)$ and $f(\theta_R,E)$ are well behaved]. Thus, in a numerical calculation, we only expect $f(\theta_R,t)$ to be significantly different from zero for $0 < t < t_{max}$, where t_{max} is a time at which the reaction has finished and AB and C are no longer interacting.

Since $F(E)$ is dimensionless, eq 2.2 shows that $f(\theta_R,t)$ has dimensions of *length* × *energy*, unlike $f(\theta_R,E)$ which has the usual dimensions of *length*. However to keep the notation simple, we use the same symbol f for the different functions $f(\theta_R,E)$ and $f(\theta_R,t)$ and distinguish them by their differing arguments. This convention is also adopted in the paper for other physical quantities in the energy and time domains.

By analogy with the differential cross section, eq 2.1, we also define

$$\sigma(\theta_R,t) = |f(\theta_R,t)|^2 \qquad (2.3)$$

Since $\sigma(\theta_R,t)$ has dimensions of *length*^{2} × *energy*^{2} rather than *length*^{2}, we will not call $\sigma(\theta_R,t)$ a "time-dependent differential cross section"; instead, we will use the terms "time-dependent angular distribution" or "time-dependent scattering pattern".

The inverse Fourier transform of eq 2.2 is

$$f(\theta_R,E) = \frac{1}{2\pi\hbar F(E)} \int_0^\infty f(\theta_R,t) \exp(iEt/\hbar)\, dt \qquad \text{(N.B., dimensions = length)} \quad (2.4)$$

Equation 2.4 can be used in an alternative formulation of the theory in which the starting point is $f(\theta_R,t)$.[11−13] In the limit, $E \rightarrow \infty$, the integral in eq 2.4 will tend to zero by the Riemann−Lebesgue lemma[50] [assuming $f(\theta_R,t)$ is well behaved]. However, in this limit we also have $F(E) \rightarrow 0$, resulting in the indeterminate form 0/0 and a more detailed investigation is necessary to find the limiting behavior of $f(\theta_R,E)$.

It is well-known there is no universal convention in the literature for a Fourier transform and its inverse. In our derivations above and below, the following form is convenient to use. If

$$G(t) = \frac{1}{(2\pi\hbar)^{1/2}} \int_{-\infty}^\infty g(E) \exp(-iEt/\hbar)\, dE \qquad (2.5)$$

then

$$g(E) = \frac{1}{(2\pi\hbar)^{1/2}} \int_{-\infty}^\infty G(t) \exp(iEt/\hbar)\, dt \qquad (2.6)$$

C. Cumulative Time-Evolving Differential Cross Section. We next define a cumulative time-evolving scattering amplitude by modifying eq 2.4 to

$$f_t(\theta_R,E) = \frac{1}{2\pi\hbar F(E)} \int_0^t f(\theta_R,t') \exp(iEt'/\hbar)\, dt' \qquad \text{(N.B., dimensions = length)} \quad (2.7)$$

The corresponding cumulative time-evolving differential cross section is then

$$\sigma_t(\theta_R,E) = |f_t(\theta_R,E)|^2 \quad (2.8)$$

Note that $f_t(\theta_R,E) \rightarrow f(\theta_R,E)$ and $\sigma_t(\theta_R,E) \rightarrow \sigma(\theta_R,E)$ as $t \rightarrow \infty$. The definitions (2.7) and (2.8) allow us to see how features in $\sigma(\theta_R,E)$ arise as $\sigma_t(\theta_R,E)$ evolves from $t = 0$ to $t = \infty$. In particular, if $\sigma_t(\theta_R,E)$ is plotted at different time steps, we can create a movie in which each frame corresponds to each time step and hence see visually how $\sigma_t(\theta_R,E)$ evolves as $t \rightarrow \infty$ (in practice to $t = t_{max}$).

It is important to note that $f_t(\theta_R,E)$ and $\sigma_t(\theta_R,E)$ should *not* be interpreted as the scattering amplitude and differential cross section respectively at a fixed time t and a fixed energy E, as this would contradict the energy−time uncertainty relation.[51] In fact $f_t(\theta_R,E)$ contains contributions from many energies. This can be seen by substituting eq 2.2 into eq 2.7, which gives

$$f_t(\theta_R,E) = \frac{1}{2\pi\hbar F(E)}\int_0^t dt' \int_0^\infty dE' F(E') f(\theta_R,E') \exp[i(E - E')t'/\hbar] \quad (2.9)$$

When t is close to zero in eq 2.9, the exponential factor is slowly oscillating, and many energies will make a significant numerical contribution to the rhs. As t increases, the exponential factor oscillates faster and the contributing energies become concentrated around $E' = E$, until for $t \rightarrow \infty$ the integrand becomes proportional to a delta function in $E' - E$ and the only contributing energy is $E' = E$.

D. Cumulative Energy-Evolving Angular Distribution. In a similar way, we can use eq 2.2 to define a cumulative energy-evolving scattering amplitude

$$f_E(\theta_R,t) = \int_0^E F(E') f(\theta_R,E') \exp(-iE't/\hbar)\, dE' \quad \text{(N.B., dimensions = length × energy)} \quad (2.10)$$

and a cumulative energy-evolving angular distribution

$$\sigma_E(\theta_R,t) = |f_E(\theta_R,t)|^2 \quad (2.11)$$

We could use eqs 2.10 and 2.11 to study how $\sigma_E(\theta_R,t)$ evolves in energy from $E = 0$ to $E = E_{max}$, for example. However, this way of understanding the dynamics of chemical reactions is probably less useful than the concept of the cumulative time-evolving differential cross section described in section 2C. Note that the rhs of eq 2.11 contains contributions from a spread of times [as substituting eq 2.4 into eq 2.11 shows].

E. Partial Wave Series. In our application to the $H + D_2$ reaction in sections 3 and 4, the helicity quantum numbers m_i and m_f for the transition are both equal to zero. This means that $f(\theta_R,E)$ can be expanded in a basis set of Legendre polynomials. We can write

$$f(\theta_R,E) = \frac{1}{2ik(E)}\sum_{J=0}^{\infty}(2J+1)S_J(E)P_J(\cos(\pi - \theta_R))$$

or

$$f(\theta_R,E) = \frac{1}{2ik(E)}\sum_{J=0}^{\infty}(2J+1)\tilde{S}_J(E)P_J(\cos\theta_R) \quad (2.12)$$

where $k(E)$ is the initial translational wavenumber, J is the total angular momentum quantum number, $\tilde{S}_J(E) = \exp(i\pi J)S_J(E)$ is a modified energy-dependent scattering matrix element and $P_J(\bullet)$ is a Legendre polynomial of degree J.

In a similar way, we can make a partial wave expansion for $f(\theta_R,t)$ by writing[11−13]

$$f(\theta_R,t) = \frac{1}{2i}\sum_{J=0}^{\infty}(2J+1)\tilde{S}_J(t)P_J(\cos\theta_R) \quad (2.13)$$

where $\tilde{S}_J(t)$ is a modified time-dependent scattering matrix element [N.B., no $k(E)$ on the rhs of eq 2.13]. Substituting eqs 2.12 and 2.13 into eq 2.2 leads to

$$\tilde{S}_J(t) = \int_0^\infty \frac{F(E)}{k(E)}\tilde{S}_J(E)\exp(-iEt/\hbar)\, dE \quad \text{(N.B., dimensions = length × energy)} \quad (2.14)$$

Using eqs 2.5 and 2.6, the inverse Fourier transformation of eq 2.14 is

$$\tilde{S}_J(E) = \frac{1}{2\pi\hbar}\frac{k(E)}{F(E)}\int_0^\infty \tilde{S}_J(t)\exp(iEt/\hbar)\, dt \quad \text{(N.B., dimensionless)} \quad (2.15)$$

We can also define cumulative energy-evolving and cumulative time-evolving scattering matrix elements by replacing the infinite upper limits in eqs 2.14 and 2.15 by E and t respectively. For example

$$\tilde{S}_J^{(t)}(E) = \frac{1}{2\pi\hbar}\frac{k(E)}{F(E)}\int_0^t \tilde{S}_J(t')\exp(iEt'/\hbar)\, dt' \quad \text{(N.B., dimensionless)} \quad (2.16)$$

with $\tilde{S}_J^{(\infty)}(E) \equiv \tilde{S}_J(E)$. The cumulative time-evolving scattering amplitude, $f_t(\theta_R,E)$, is then given by the partial wave expansion

$$f_t(\theta_R,E) = \frac{1}{2ik(E)}\sum_{J=0}^{\infty}(2J+1)\tilde{S}_J^{(t)}(E)P_J(\cos\theta_R) \quad (2.17)$$

F. Nearside—Farside Theory. It is often found that $\sigma(\theta_R,E)$, when plotted vs θ_R at a fixed E, possesses a complicated interference structure, which contains important information on the reaction dynamics. A common difficulty in trying to understand the physical origin of this interference structure is that the partial wave series (eq 2.12) contains a large number of numerically significant terms under semiclassical conditions. In this situation, it can be helpful to apply a nearside−farside (NF) decomposition to $f(\theta_R,E)$.[19−40]

We now show that NF theory can also be applied to $f(\theta_R,t)$ and hence used to provide physical insight into structure seen in $\sigma(\theta_R,t)$ when it is plotted vs θ_R at fixed values of t.

The NF decomposition of $f(\theta_R,t)$ is given by[19−40]

$$f(\theta_R,t) = f_N(\theta_R,t) + f_F(\theta_R,t) \quad (2.18)$$

where the NF time-dependent subamplitudes are

$$f_{N,F}(\theta_R,t) = \frac{1}{2i}\sum_{J=0}^{\infty}(2J+1)\tilde{S}_J(t)Q_J^{(\mp)}(\cos\theta_R) \quad (2.19)$$

with $(\theta_R \neq 0,\pi)$

$$Q_J^{(\mp)}(\cos\theta_R) = \frac{1}{2}\left[P_J(\cos\theta_R) \pm \frac{2i}{\pi}Q_J(\cos\theta_R)\right] \quad (2.20)$$

and $Q_J(\cos\theta_R)$ is a Legendre function of the second kind of degree J. The corresponding NF time-dependent angular distributions are $(\theta_R \neq 0,\pi)$

$$\sigma_{N,F}(\theta_R,t) = |f_{N,F}(\theta_R,t)|^2 \quad (2.21)$$

In many cases, $\sigma_N(\theta_R,t)$ or $\sigma_F(\theta_R,t)$ vary more slowly with θ_R (at a fixed t) than does $\sigma(\theta_R,t)$, which enables one to identify angular regions of N or F dominance or regions where there is NF interference. The results of a NF decomposition for $f(\theta_R,t)$ are reported in section 4 at four values of t.

G. Local Angular Momentum Analysis. Local angular momentum (LAM) analysis is a new procedure for extracting physical information from a partial wave series.[35,36,38,40] The LAM is the value of the total angular momentum variable that mainly contributes to the scattering at a given θ_R. For $f(\theta_R,E)$, it is defined by[35,36,38,40]

$$\mathrm{LAM}(\theta_R,E) = \frac{\mathrm{d}(\arg f(\theta_R,E))}{\mathrm{d}\theta_R} \quad (2.22)$$

where the arg in eq 2.22 is not necessarily the principal value in order that the derivative be well-defined. By analogy with eq 2.22, we can define a LAM for $f(\theta_R,t)$: it is given by

$$\mathrm{LAM}(\theta_R,t) = \frac{\mathrm{d}(\arg f(\theta_R,t))}{\mathrm{d}\theta_R} \quad (2.23)$$

In general, $\mathrm{LAM}(\theta_R,t) \notin \{J = 0,1,2,...\}$; instead, $\mathrm{LAM}(\theta_R,t)$ is real (positive or negative).

It is found in section 4 that $\mathrm{LAM}(\theta_R,t)$ often possesses a complicated interference pattern when plotted against θ_R at fixed t. It is then useful to define N and F LAMs for the N and F subamplitudes, respectively. We have

$$\mathrm{LAM}_{N,F}(\theta_R,t) = \frac{\mathrm{d}(\arg f_{N,F}(\theta_R,t))}{\mathrm{d}\theta_R} \quad (2.24)$$

Positive values of $\mathrm{LAM}(\theta_R,t)$ can be identified with the anticlockwise motion of travelling angular waves around the reaction zone and negative values to their clockwise motion.[35,36,38,40] This means that positive and negative $\mathrm{LAM}(\theta_R,t)$ values can be attributed to F and N dominance, respectively, and in general to attractive and repulsive forces, respectively. This leads to a useful property of a NF LAM analysis: it should in general be consistent with, and in certain cases clarify, the findings of a NF analysis of the angular distributions, as already described in section 2F.

3. Calculations

We performed scattering calculations for the state-to-state reaction, $H + D_2(v_i = 0, j_i = 0, m_i = 0) \rightarrow HD(v_f = 3, j_f = 0, m_f = 0) + D$, using the potential energy surface number 2 of Boothroyd et al.[52] with masses of $m_H = 1.008$ u and $m_D = 2.014$ u. First, we computed $\tilde{S}_J(E)$ for $J = 0$ (1) 30 on the energy grid, $E = 1.52(0.01)2.50$ eV. Here E is measured with respect to the classical minimum of the D_2 potential energy curve. Since the rovibrational energy, $E(v_i,j_i)$, of $D_2(v_i = 0, j_i = 0)$ is 0.192 eV and the rovibrational energy, $E(v_f,j_f)$, of $HD(v_f = 3, j_f = 0)$ is 1.520 eV, the reaction is closed for $E < 1.520$ eV. The energy-domain scattering matrix elements were computed by a state-to-state wave packet method developed by one of us.[53] In particular, the reactant-product decoupling equations were solved in a form that partitions the Schrödinger equation for reactive scattering into reactant, strong interaction and product regions. This method has been applied to a variety of chemical reactions in refs 6−10, 12, 18, and 53−58.

Second, we interpolated the modulus and phase of $\tilde{S}_J(E)$ and then evaluated $\tilde{S}_J(t)$ numerically from the half-Fourier transform (eq 2.14) for the time grid 0, 0.48 (0.68), 150 fs. The filter function, $F(E)$, is given by[11,12]

$$F(E) = \frac{1}{2\sqrt{2\pi}} g(E) \exp\{\mathrm{i}[k_i(E)z_i + k_f(E)z_f]\} \quad (2.25)$$

where $k_i(E)$ and z_i are the initial translational wavenumber and distance, respectively, and likewise for the final quantities, $k_f(E)$, z_f. We set $z_i = 6\ a_0$ in eq 2.25; this value localizes the center of the initial PWP at a distance of $-6\ a_0$ on the z axis with a width determined by $|F(E)|$. In addition, we used the value $z_f = 6\ a_0$ which distributes the centers of the probe PWPs around a sphere of radius $6\ a_0$ in the exit channel. In addition, $k_s(E) = \{2\mu_{X,YZ}[E - E(v_s,j_s)]\}^{1/2}/\hbar$, with s = i, f where $\mu_{X,YZ} = m_X(m_Y + m_Z)/(m_X + m_Y + m_Z)$ is the reduced mass of the X + YZ channel. The function, $g(E)$ is a distributed approximating functional (DAF) defined by[11,12]

$$g(E) = \exp(-\bar{E}^2)\sum_{m=0}^{M/2} \bar{E}^{2m}/m!, \quad \bar{E}^2 = \frac{1}{2}(E - E_0)^2\sigma^2$$

with parameters $M = 88$, $E_0 = 1.65$ eV, and $\sigma = 1/0.07$ eV^{-1}, which is a constant not related to the cross section. This DAF is approximately unity from the opening of the reaction channel at $E = 1.520$ eV to $E = 2.2$ eV when it decreases monotonically to approximately 10^{-4} at $E = 2.5$ eV. As an additional check on our numerics, we regenerated $\{\tilde{S}_J(E)\}$ by applying the inverse Fourier transform (eq 2.15) to the $\{\tilde{S}_J(t)\}$.

Finally we calculated the full and NF time-dependent scattering amplitudes from their partial wave series representations, eqs 2.13 and 2.19. The full and NF time-dependent LAMs are then obtained from eq 2.23 and 2.24 respectively, with the full and NF time-dependent angular distributions being given by eqs 2.3 and 2.21 respectively. The cumulative time-evolving scattering amplitude, (2.7), also requires an additional quadrature over time in order to compute the cumulative time-evolving differential cross section, (2.8). We found it convenient to use the partial wave representation, eqs 2.16 and 2.17, to accomplish this, by numerically evaluating the $\tilde{S}_J^{(t)}(E)$ for $J = 0$, 1, 2, ..., 30 at different times t.

4. Results

A. NF Analysis of Time-Dependent Angular Distributions. Perspective plots of $\sigma(\theta_R,t)\sin\theta_R$ and $\sigma_{N,F}(\theta_R,t)\sin\theta_R$ are shown in Figure 1 from $t = 0$ fs to $t = 99.5$ fs. The angular distributions have been multiplied by $\sin\theta_R$ in order to contain large features in the scattering[6,7] close to $\theta_R = 0°$ and $\theta_R = 180°$. Time slices of Figure 1 for the logarithm of the full and NF angular distributions at $t = 29.8$, 50.3, 70.1, and 102.2 fs are displayed in Figure 2 (N.B., no $\sin\theta_R$ factor).

Figure 1 shows that the reaction starts at $t \approx 20$ fs with a large peak appearing at backward angles for $t \approx 35$ fs. As t increases, the backward peak disappears and the scattering moves toward the forward direction, with a large oscillatory peak being present for $t \approx 60$ fs, i.e., a time delay of about 25 fs relative to the direct scattering. As t increases further, the forward peak also disappears and the reaction is essentially over by $t = 99.5$ fs. The perspective plots for $t > 99.5$ fs to $t = 150$ fs look the same as those for $t = 99.5$ fs.

Figure 2a shows that the backward peak at $t = 29.8$ fs is N dominated. This is the expected behavior for direct (i.e., short-time) reaction dynamics. Indeed, an approximate N theory, the

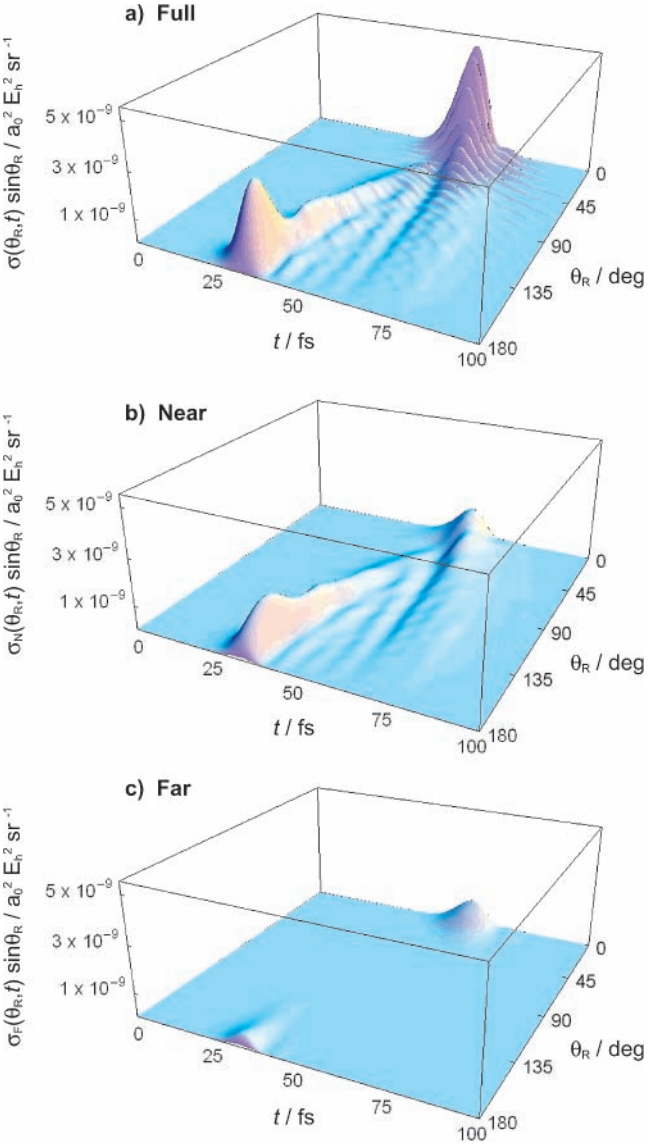

Figure 1. Perspective plots of (a) $\sigma(\theta_R,t)$ sin θ_R, (b) $\sigma_N(\theta_R,t)$ sin θ_R, and (c) $\sigma_F(\theta_R,t)$ sin θ_R vs θ_R and t. The plots for $t > 99.5$ fs to $t = 150$ fs look the same as those for $t = 99.5$ fs.

semiclassical optical model,[21,29,34] has successfully reproduced the backward angle scattering in fixed-energy differential cross sections for several simple reactions, including H + D_2.[29]

Figures 1c and 2a suggest that the F subamplitude, although smaller in magnitude than the N subamplitude, also makes a nonnegligible contribution to the scattering at backward angles. However, this is likely to be a (well-understood) example[25] of the NF decomposition overestimating the F contribution at backward angles. The overestimation arises because the NF cross sections diverge logarithmically as $\theta_R \rightarrow 180°$. This causes the F angular distribution to increase in the backward direction rather than to decrease, and as a consequence, for $154° \lesssim \theta_R \lesssim 178°$, the N angular distribution is reduced in magnitude, before it too diverges for $\theta_R \gtrsim 178°$. We have found that a resummation[35,36,38] of the partial wave series (eq 2.13) "cleans" the NF curves in Figure 2a of nonphysical oscillations, thereby improving the usefulness of the NF decomposition; this will be illustrated and discussed in a future paper.

Parts a and b of Figure 2 show that the situation is quite different for the large time-delayed peak at forward angles where the N and F angular distributions vary relatively slowly with

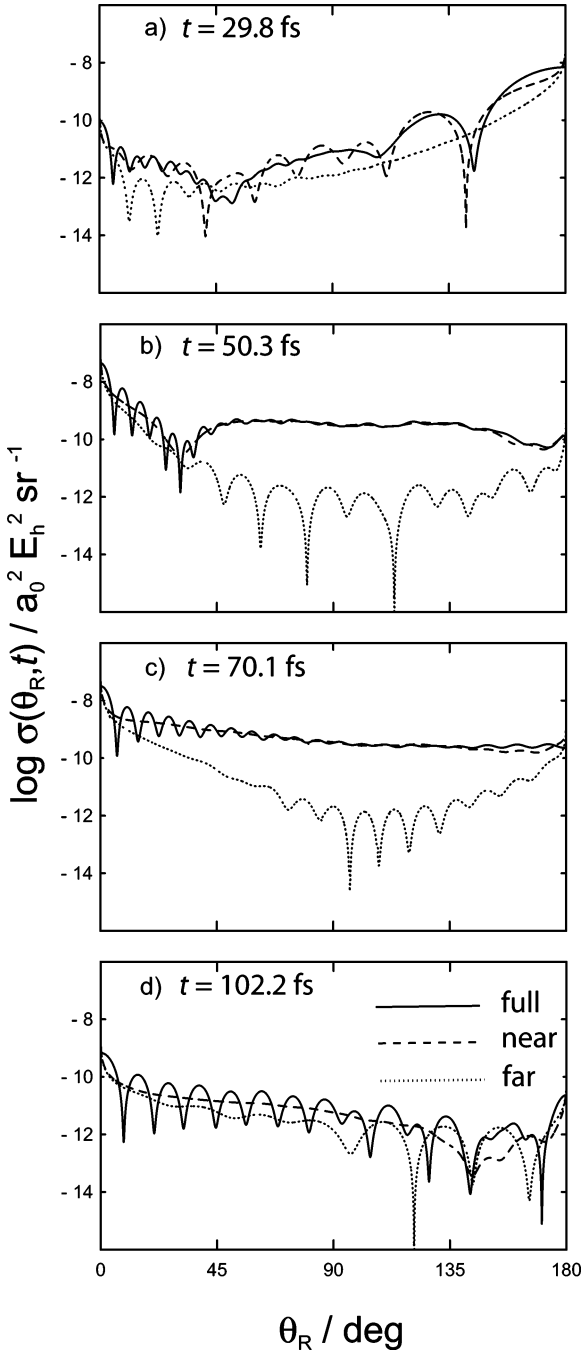

Figure 2. Logarithmic plots of $\sigma(\theta_R,t)$ (solid line), $\sigma_N(\theta_R,t)$ (dashed line), and $\sigma_F(\theta_R,t)$ (dotted line) vs θ_R for (a) $t = 29.8$ fs, (b) $t = 50.3$ fs, (c) $t = 70.1$ fs, and (d) $t = 102.2$ fs.

θ_R: it is NF interference between the NF subamplitudes that gives rise to the pronounced oscillations in the forward direction. It is likely this oscillatory forward angle scattering can be interpreted as a *glory*, since a uniform semiclassical analysis[37,39,40] has proven[37,46] that a forward glory is present in $\sigma(\theta_R,E)$ at $E = 2.00$ eV.

At $t = 102.2$ fs, Figures 1 and 2d demonstrate that the full and NF angular distributions have become very small in magnitude and the reaction is largely over. Nevertheless the full cross section, although small, still possesses regular oscillations, in the forward direction, which clearly arise from NF interference.

B. LAM Analysis of Time-Dependent Scattering Amplitudes. Figure 3 shows plots of LAM(θ_R,t) and $\text{LAM}_{N,F}(\theta_R,t)$ for the same times as Figure 2, namely $t = 29.8$, 50.3, 70.1,

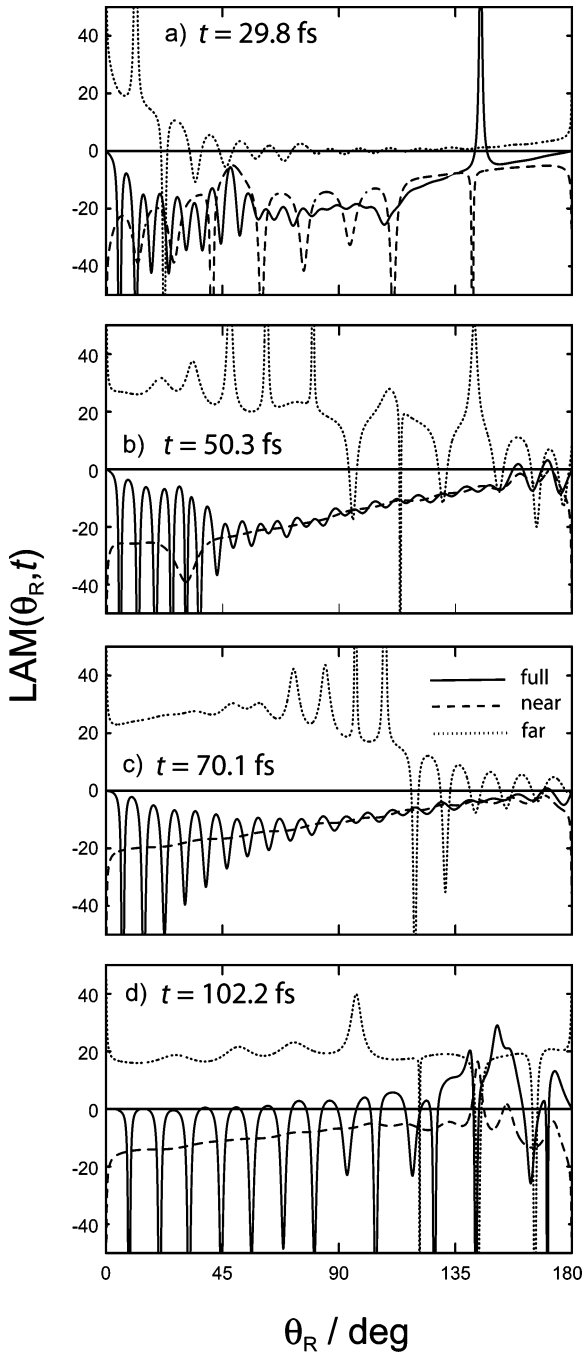

Figure 3. Plots of $LAM(\theta_R,t)$ (solid line), $LAM_N(\theta_R,t)$ (dashed line), and $LAM_N(\theta_R,t)$ (dotted line) vs θ_R for (a) $t = 29.8$ fs, (b) $t = 50.3$ fs, (c) $t = 70.1$ fs, and (d) $t = 102.2$ fs.

102.2 fs. At the first time, $t = 29.8$ fs, the full $LAM(\theta_R,t)$ is negative at most angles and so the scattering is N dominated. An exception is a small angular region around $\theta_R = 145°$, where $LAM(\theta_R,t)$ becomes positive. There is similar behavior at the three other times, with the scattering usually being N dominated. Notice that $LAM_N(\theta_R,t)$ and $LAM_F(\theta_R,t)$ generally vary more slowly with θ_R than does $LAM(\theta_R,t)$. Thus, the regular oscillations present in $LAM(\theta_R,t)$ at forward angles are usually caused by NF interference. The above LAM interpretation is confirmed by a resummation[35,36,38] of the partial wave series (2.13) which, as for the NF angular distributions, "cleans" the NF LAM curves of nonphysical oscillations. When viewing Figure 3, it should also be remembered[35,36,40] that a F LAM loses its physical significance in angular regions where $\sigma_F(\theta_R,t)$ is negligible compared to $\sigma(\theta_R,t)$. On comparing Figures 2 and

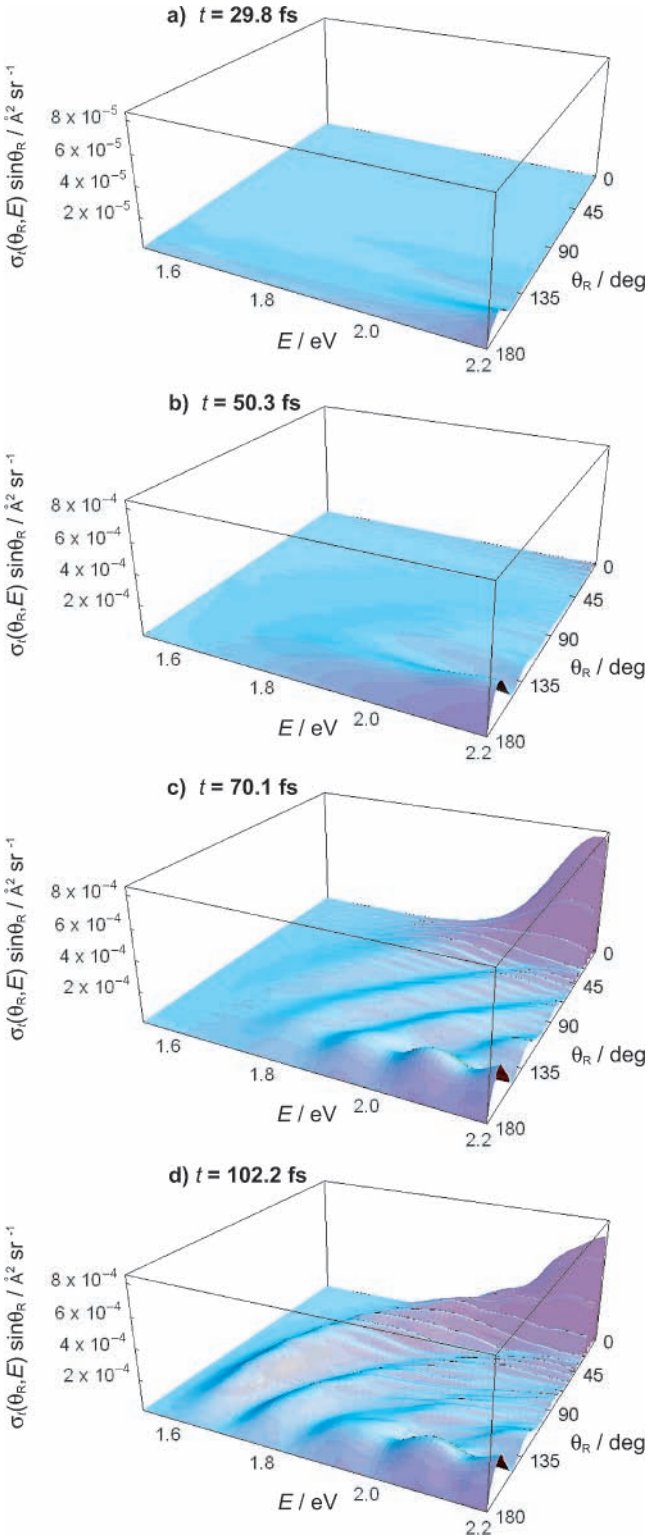

Figure 4. Plots of $\sigma_t(\theta_R,E)$ sin θ_R vs E and θ_R for (a) $t = 29.8$ fs, (b) $t = 50.3$ fs, (c) $t = 70.1$ fs, and (d) $t = 102.2$ fs. Note that the scale along the z-axis of plot a is smaller than the scales of plots b−d, to allow a more detailed view of the structure.

3, we see that the NF LAM results are consistent with the NF analyses of the angular distributions. An advantage of the LAM analysis is that it is easier to identify angular regions of N or F dominance, when these are less apparent in the angular distributions.

Parts b−d of Figure 3 show that the $LAM_N(\theta_R,t)$ curves decrease in magnitude, roughly monotonically, as θ_R increases toward 180°. This is the behavior expected for direct repulsive

interactions of the hard-sphere type. Indeed the N LAMs can be approximately fitted by the classical-mechanical hard-sphere relation, $LAM_N(\theta_R,t) = -LAM_{max} \cos(\theta_R/2)$. In contrast, the $LAM_F(\theta_R,t)$ curves are approximately constant at forward scattering angles, with values in the range 26.0−26.8 for Figure 3b and 23.0−27.6 for Figure 3c; i.e., the NF LAM analysis has identified these ranges of J values as being dynamically important for forward scattering. Inspection of graphs of $|\tilde{S}_J(t)|$ vs J shows that these J values correspond to high-J shoulders on the $|\tilde{S}_J(t)|$ plots. These findings are similar to a NF LAM analysis of the F + H_2($v_i = 0$, $j_i = 0$, $m_i = 0$) FH($v_f = 3$, $j_f = 3$, $m_f = 0$) + H reaction at $E = 0.3872$ eV, which also identified a high-J shoulder on the $|\tilde{S}_J(E)|$ graph as being dynamically important for the forward angle scattering.[38]

C. Cumulative Time-Evolving Differential Cross Section. Figure 4 shows perspective plots of four snapshots taken from a movie of the cumulative time-evolving differential cross section, $\sigma_t(\theta_R,E)$, for the same values of t used in Figures 2 and 3 [N.B., $\sigma_t(\theta_R,E)$ has been multiplied by sin θ_R, cf., Figure 1]. At the first time, $t = 29.8$ fs, the time-direct mechanism is starting to be visible at backward angles, although $\sigma_t(\theta_R,E)$ is still small. By $t = 50.3$ fs, the direct mechanism is more clearly visible in the snapshot and the time-delayed scattering is starting to appear, causing small oscillations in $\sigma_t(\theta_R,E)$. At $t = 70.1$ fs, most of the structures are present, with the forward peak displaying glorylike oscillations. In the final snapshot at $t = 102.2$ fs, the reaction is almost over and $\sigma_t(\theta_R,E)$ is in good agreement with the energy domain $\sigma(\theta_R,E)$, shown in Figure 2 of ref 6 and in Figure 3 of ref 7. Ridges similar to those in Figure 4d were originally discussed by Continetti et al.[59] (for D + H_2), by Miller and Zhang[60] [for H(D) + H_2], and by Aoiz et al.[61,62] (for D + H_2).

5. Conclusions

We have applied NF and LAM techniques, originally developed for the analysis of collisions at fixed total energies, to the PWP theory of time-dependent scattering. This was possible because the PWP theory employs concepts and formulas analogous to those found in time-independent scattering theory; in particular the PWP theory uses time-dependent scattering matrix elements, scattering amplitudes and angular distributions.

We studied the H + D_2 reaction because it exhibits two distinct collision mechanisms, separated in time by about 25 fs. We found N dominance for the time-direct mechanism, where the products scatter into backward angles, whereas there are NF interference effects in the time-delayed mechanism, which possesses a large oscillatory forward peak.

We introduced the concepts of a cumulative time-evolving differential cross section and a cumulative energy evolving angular distribution. We showed that snapshots from a movie of the cumulative time-evolving differential cross section provide an alternative understanding of the time-direct and time-delayed mechanisms.

Acknowledgment. Support of this research by the U.K. Engineering and Physical Sciences Research Council is gratefully acknowledged.

References and Notes

(1) Aoiz, F. J.; Bañares, L.; Herrero, V. J. *Int. Rev. Phys. Chem.* **2005**, *24*, 119.

(2) *Theory of Chemical Reaction Dynamics*; Proceedings of the NATO Advanced Research Workshop on Theory of the Dynamics of Elementary Chemical Reactions, Balatonföldár, Hungary, 8−12 June, 2003; Laganà, A.; Lendvay, G., Eds.; Kluwer: Dordrecht: The Netherlands, 2004.

(3) *Modern Trends in Chemical Reaction Dynamics, Experiment and Theory*; Yang. X., Liu, K., Eds.; World Scientific: Singapore, 2004; Parts I and II.

(4) Althorpe, S. C.; Clary, D. C. *Annu. Rev. Phys. Chem.* **2003**, *54*, 493.

(5) Nyman, G.; Yu, H.-G. *Rep. Prog. Phys.* **2000**, *63*, 1001.

(6) Althorpe, S. C.; Fernández-Alonso, F.; Bean, B. D.; Ayers, J. D.; Pomerantz, A. E.; Zare, R. N.; Wrede, E. *Nature (London)* **2002**, *416*, 67.

(7) Althorpe, S. C. *J. Chem. Phys.* **2002**, *117*, 4623.

(8) Althorpe, S. C. *Chem. Phys. Lett.* **2003**, *370*, 443.

(9) Althorpe, S. C. *J. Phys. Chem. A* **2003**, *107*, 7152.

(10) Juanes-Marcos, J. C.; Althorpe, S. C. *Chem. Phys. Lett.* **2003**, *381*, 743.

(11) Althorpe, S. C. *Phys. Rev. A* **2004**, *69*, 042702.

(12) Althorpe, S. C. *J. Chem. Phys.* **2004**, *121*, 1175.

(13) Althorpe, S. C. *Int. Rev. Phys. Chem.* **2005**, *23*, 219.

(14) Neuhauser, D.; Baer, M.; Judson, R. S.; Kouri, D. J. *J. Chem. Phys.* **1989**, *90*, 5882.

(15) Peng, T.; Zhang, J. Z. H. *J. Chem. Phys.* **1996**, *105*, 6072.

(16) Kouri, D. J.; Hoffman, D. K. *Few-Body Syst.* **1995**, *18*, 203.

(17) Kouri, D. J.; Huang, Y.; Zhu, W.; Hoffman, D. K. *J. Chem. Phys.* **1994**, *100*, 3662.

(18) Juanes-Marcos, J. C.; Althorpe, S. C.; Wrede, E. *Science* **2005**, *309*, 1227. For a commentary, see: Clary, D. C. *Science* **2005**, *309*, 1195.

(19) Connor, J. N. L.; McCabe, P.; Sokolovski, D.; Schatz, G. C. *Chem. Phys. Lett.* **1993**, *206*, 119.

(20) Sokolovski, D.; Connor, J. N. L.; Schatz, G. C. *Chem. Phys. Lett.* **1995**, *238*, 127.

(21) Sokolovski, D.; Connor, J. N. L.; Schatz, G. C. *J. Chem. Phys.* **1995**, *103*, 5979.

(22) McCabe, P.; Connor, J. N. L. *J. Chem. Phys.* **1996**, *104*, 2297.

(23) Sokolovski, D.; Connor, J. N. L.; Schatz. G. C. *Chem. Phys.* **1996**, *207*, 461.

(24) Wimp, J.; McCabe, P.; Connor, J. N. L. *J. Comput. Appl. Math.* **1997** *82*, 447.

(25) McCabe, P.; Connor, J. N. L.; Sokolovski, D. *J. Chem. Phys.* **1998**, *108*, 5695.

(26) Sokolovski, D.; Connor, J. N. L. *Chem. Phys. Lett.* **1999**, *305*, 238.

(27) Hollifield, J. J.; Connor, J. N. L. *Phys. Rev. A* **1999**, *59*, 1694.

(28) Hollifield, J. J.; Connor, J. N. L. *Mol. Phys.* **1999**, *97*, 293.

(29) Dobbyn, A. J.; McCabe, P.; Connor, J. N. L.; Castillo, J. F. *Phys. Chem. Chem. Phys.* **1999**, *1*, 1115.

(30) Vrinceanu, D.; Msezane, A. Z.; Bessis, D.; Connor, J. N. L.; Sokolovski, D. *Chem. Phys. Lett.* **2000**, *324*, 311.

(31) McCabe, P.; Connor, J. N. L.; Sokolovski, D. *J. Chem. Phys.* **2001**, *114*, 5194.

(32) Whiteley, T. W. J.; Noli, C.; Connor, J. N. L. *J. Phys. Chem. A* **2001**, *105*, 2792.

(33) Noli, C.; Connor, J. N. L.; Rougeau, N.; Kubach, C. *Phys. Chem. Chem. Phys.* **2001**, *3*, 3946.

(34) Noli, C.; Connor, J. N. L. *Russ. J. Phys. Chem.* **2002**, *76* (Supplement 1), S77. Also available at: http://arXiv.org/abs/physics/0301054.

(35) Anni, R.; Connor, J. N. L.; Noli, C. *Phys. Rev. C* **2002**, *66*, 044610.

(36) Anni, R.; Connor, J. N. L.; Noli, C. *Khim. Fiz.* **2004**, *23*, No 2, 6. Also available at: http://arXiv.org/abs/physics/0410266.

(37) Connor, J. N. L. *Phys. Chem. Chem. Phys.* **2004**, *6*, 377.

(38) Connor, J. N. L.; Anni, R. *Phys. Chem. Chem. Phys.* **2004**, *6*, 3364.

(39) Connor. J. N. L. *Mol. Phys.* **2005**, *103*, 1715; in ref 21 of this paper, for "P. McCabe", read "G. C. Schatz".

(40) Xiahou, C.; Connor, J. N. L. *Mol. Phys.* **2006**, in press.

(41) Sokolovski, D.; Castillo, J. F.; Tully, C. *Chem. Phys. Lett.* **1999**, *313*, 225.

(42) Sokolovski, D.; Castillo, J. F. *Phys. Chem. Chem. Phys.* **2000**, *2*, 507.

(43) Sokolovski, D. *Phys. Rev. A* **2000**, *62*, 024702.

(44) Aoiz, F. J.; Bañares, L.; Castillo, J. F.; Sokolovski, D. *J. Chem. Phys.* **2002**, *117*, 2546.

(45) Sokolovski, D. *Russ. J. Phys. Chem.* **2002**, *76* (Supplement 1), S21.

(46) Sokolovski, D. *Chem. Phys. Lett.* **2003**, *370*, 805.

(47) Sokolovski, D.; Msezane, A. Z. *Phys. Rev. A* **2004**, *70*, 032710.

(48) Schatz, G. C. In *Advances in Classical Trajectory Methods*; Hase, W. L., Ed.; JAI Press: Stamford, CT, 1998; Vol. 3, pp 205−229.

(49) Harich, S. A.; Dai, D.; Wang, C. C.; Yang, X.; Chao, S. S.; Skodje, R. T. *Nature (London)* **2002**, *419*, 281. For a commentary, see: Manolopoulos, D. E. *Nature* **2002**, *419*, 266.

(50) *Fourier and Laplace Transforms*; Beerends, R. J., ter Morsche, H. G., van den Berg, J. C., van de Vrie, E. M., Eds.; translated from the Dutch by Beerends, R. J.; Cambridge University Press: Cambridge, U.K., 2003; p 165.

(51) *Quantum Mechanics*; Messiah, A.; translated from the French by Temmer, G. M.; North-Holland: Amsterdam, The Netherlands, 1961; Vol. I, pp 135−138, 319, 320, 447.

(52) Boothroyd, A. I.; Keogh, W. J.; Martin, P. G.; Peterson, M. R. *J. Chem. Phys.* **1996**, *104*, 7139.

(53) Althorpe, S. C. *J. Chem. Phys.* **2001**, *114*, 1601.

(54) Pomerantz, A. E.; Ausfelder, F.; Zare, R. N.; Althorpe, S. C.; Aoiz, F. J.; Bañares, L.; Castillo, J. F. *J. Chem. Phys.* **2004**, *120*, 3244.

(55) Ausfelder, F.; Pomerantz, A. E.; Zare, R. N.; Althorpe, S. C.; Aoiz, F. J.; Bañares, L.; Castillo, J. F. *J. Chem. Phys.* **2004**, *120*, 3255.

(56) Pomerantz, A. E.; Ausfelder, F.; Zare, R. N.; Juanes-Marcos, J. C.; Althorpe, S. C.; Sáez Rábanos, V.; Aoiz, F. J.; Bañares, L.; Castillo, J. F. *J. Chem. Phys.* **2004**, *121*, 6587.

(57) Juanes-Marcos, J. C.; Althorpe, S. C. *J. Chem. Phys.* **2005**, *122*, 204324.

(58) Koszinowski, K.; Goldberg, N. T.; Pomerantz, A. E.; Zare, R. N. Juanes-Marcos, J. C.; Althorpe, S. C. *J. Chem. Phys.* **2005**, *123*, 054306.

(59) Continetti, R. E.; Zhang, J. Z. H.; Miller, W. H. *J. Chem. Phys.* **1990**, *93*, 5356.

(60) Miller, W. H.; Zhang, J. Z. H. *J. Phys. Chem.* **1991**, *95*, 12.

(61) Aoiz, F. J.; Herrero, V. J.; Sáez Rábanos, V. *J. Chem. Phys.* **1991**, *95*, 7767.

(62) Aoiz, F. J.; Herrero, V. J.; Sáez Rábanos, V. *J. Chem. Phys.* **1992**, *97*, 7423.